HHS Public Access

Author manuscript

Can J Ophthalmol. Author manuscript; available in PMC 2023 August 01.

Published in final edited form as:

Can J Ophthalmol. 2022 August ; 57(4): 217–227. doi:10.1016/j.jcjo.2021.04.025.

Advances in magnetic resonance imaging of orbital disease

Rebecca E. Tanenbaum, MD[1], **Remy Lobo, MD**[2], **Alon Kahana, MD, PhD**[3,4], **Sara T. Wester, MD**[1]

[1]Bascom Palmer Eye Institute, Department of Ophthalmology, University of Miami Miller School of Medicine, Miami, Florida

[2]Department of Radiology, University of Michigan, Ann Arbor, Michigan

[3]Department of Ophthalmology, Oakland University William Beaumont School of Medicine, Rochester, Michigan

[4]Consultants in Ophthalmic and Facial Plastic Surgery, Southfield, Michigan

Abstract

Magnetic resonance imaging (MRI) is increasingly used by the orbital surgeon to aid in the diagnosis, surgical planning, and monitoring of orbital disease. MRI provides superior soft tissue detail compared to computed tomography or ultrasound, and advancing techniques enhance its ability to highlight abnormal orbital pathology. Diffusion-weighted imaging is a specialized technique that uses water molecule diffusion patterns in tissue to generate contrast signal and can help distinguish malignant from benign lesions. Steady-state free precession sequences such as CISS and FIESTA generate highly detailed, three-dimensional reconstructed images, and are particularly useful in distinguishing structures adjacent to cerebral spinal fluid. Magnetic resonance angiography may be used to characterize vascular lesions within the orbit. New developments in magnetic field strength as well as the use of orbital surface coils achieve increasingly improved imaging resolution.

Keywords

orbital imaging; magnetic resonance imaging (MRI); fat suppression; STIR; diffusion-weighted imaging (DWI); dynamic contrast-enhanced (DCE) imaging; magnetic resonance angiography (MRA)

Corresponding author: Sara Tullis Wester, MD, Bascom Palmer Eye Institute, 900 NW 17th St, Miami, FL 33136, 305-326-6132, swester2@med.miami.edu.

The authors have no affiliations with or involvement in any organization or entity with any financial interest, or non-financial interest, in the subject matter or materials discussed in this manuscript.

Background

Magnetic resonance imaging (MRI) is the preferred imaging modality in many cases for the evaluation of orbital disease. In contrast to other modalities such as computed tomography (CT) or ultrasound, MRI provides superior soft tissue detail. Images are readily available in axial, coronal, and sagittal planes. Contrast enhancement and fat suppression techniques play an essential role in helping identify characteristics of abnormal processes in the orbit. Specialized imaging techniques such as diffusion-weighted imaging and dynamic contrast-enhanced imaging are helpful tools for distinguishing normal from abnormal anatomy and malignant from benign orbital lesions, e.g lymphoma from benign lymphoproliferative disease. Steady-state free precession sequences utilize repetitive excitation pulses among a steady-state magnetic field to generate highly detailed three-dimensional reconstruction of tissues that allows for precise visualization of cranial nerves and cavernous sinus lesions. Magnetic resonance angiography is particularly useful for the evaluation and characterization of vascular lesions within the orbit. Advances in MR technology provide increasingly detailed and specific information that aids in the diagnosis, pre-surgical planning, and monitoring of orbital disease.

Standard MRI protocol

Magnetic resonance technology creates images based on the alignment between polarized atomic nuclei (usually hydrogen) following excitation by a radiofrequency pulse and subsequent relaxation. The sum of magnetic moments of excited protons rotating about the axis of the magnetic field creates an MRI signal. Following excitation, T1 relaxation occurs as protons return to a resting state aligned with the external magnetic field, while T2 relaxation occurs as protons fall out of alignment with one another. T1 and T2 relaxation are determined by the properties of the atomic bonds of the area being imaged. MRI is useful in examining the soft tissues of the body as the differing properties of the atomic bonds that make up these tissues produce varying rates of T1 and T2 relaxation. The differing T1 and T2 properties inherent to tissues such as fat, water, and protein are demonstrated when MR signal information is gathered to produce an image using a mathematical process called Fourier transformation.

MRI sequences commonly used in evaluation of orbital diseases include T1 and T2, with and without fat suppression (FS), and gadolinium-enhanced T1 with fat suppression (T1+C FS). On T1, tissues with shorter T1-relaxation times, such as fat, appear brighter, or hyperintense. Tissues with high water content, such as vitreous, have longer T1-relaxation times and appear darker, or hypointense. Therefore, T1 is useful for the depiction of normal anatomical features, including fat content.

In contrast to T1, tissues with higher water content, such as vitreous or cerebrospinal fluid, have longer T2-relaxation times and appear hyperintense (bright) on T2. Hence, in general, T2 is superior in the identification of pathological features with edema (excess water content). Since fat is also bright on T2, fat suppression is employed to allow for better soft tissue contrast. On T2 FS, soft tissue edema appears hyperintense, and clearly contrasts with the hypointense appearance of fibrosis. Many pathological orbital lesions appear hyperintense on T2 FS, but paramagnetic substances containing unpaired electrons,

such as blood products, calcium, and melanin, have shortened T2 relaxation times, leading to a hypointense signal. Therefore, lesions that contain calcification (e.g. retinoblastoma, scirrhous metastases of breast carcinoma) will demonstrate intralesional hypointensities on T2.[1] The hypointense property of melanin on T2 and intrinsic T1 hyperintense signal are helpful in the identification and evaluation of choroidal melanomas, as well as intracranial melanoma metastases.

Contrast administration with gadolinium, a paramagnetic substance, is used in MRI to distinguish abnormal orbital lesions from normal tissue. The use of contrast agents (+C) improves the sensitivity of MRI by shortening the relaxation time of protons in its immediate vicinity. Thus, on T1+C, contrast-enhanced lesions will appear more hyperintense. On T2, the contrast media actually decreases signal intensity, the basis for susceptibility imaging.[2] T1+C orbital MRI can aid in highlighting focal or diffuse inflammation in the orbit. Typical radiologic characteristics of inflammatory lesions include contrast enhancement and thickening or enlargement of the involved tissue. While enhancement patterns may be nonspecific, surrounding tissue changes (fat stranding) coupled with the clinical picture (pain, erythema, edema) help differentiate inflammatory lesions from malignancy (Figure 1). Dacryoadenitis, for example, presents as enlargement of the lacrimal gland with diffuse enhancement, but signs such as blurring of the glandular margins with bordering structures and surrounding fat stranding help distinguish this as an inflammatory process over a malignant one. The pattern of contrast enhancement in a lesion can also help differentiate between inflammation, which demonstrates more homogeneous enhancement, and tumors or infection, which may appear more heterogenous in some cases due to the presence of non-enhancing components such as necrosis and pus, respectively. Extraocular muscles are characterized by low signal intensity on T1 and intermediate signal intensity on T2. Due to their rich vascular supply, they demonstrate marked enhancement following contrast administration, particularly at the periphery of the muscle. Differences in contrast enhancement due to degeneration or fibrosis of the muscle can be apparent on post-contrast T1 and may be helpful in classification of lesions.[3]

Fat suppression and STIR imaging

Fat suppression is a technique in which a saturation pulse corresponding to native fat is administered prior to the excitation pulse; this leads to the suppression of the typically high signal intensity of normal fat content. Fat suppression on T1 or T2 allows for better visualization of tissues (normal or abnormal) embedded in fat that would have been obscured by the hyperintensity of the fat signal, and therefore is particularly helpful for orbital imaging.[4] This technique also allows for the identification of fat-containing lesions in the orbit such as dermoid cysts and lipomas.[5] Fat suppression is especially important when using MRI to assess the optic nerve sheath complex, as any abnormal enhancement of the complex will be made more conspicuous when signal from surrounding orbital fat is suppressed. Close examination of this area is crucial, for example, when distinguishing optic neuritis from diseases of the optic nerve sheath. T2 FS is ideal for visualizing changes to the optic nerve and perioptic cerebrospinal fluid (CSF) in conditions that increase intracranial pressure, such as idiopathic intracranial hypertension (e.g. widened optic nerve sheath diameter, protrusion of optic nerve head into the globe) (Figure 2).[6]

In addition to clinical assessment, MRI is increasingly used as a tool to evaluate disease activity and severity. STIR (short tau inversion recovery) is a fat suppression technique in which an initial 180° inverting radiofrequency pulse is followed by a standard spin-echo sequence. The time between the two pulses can be shortened such that the signal emitted from fat is suppressed. STIR cannot be used on post-contrast T1 because of the shortening effect gadolinium has on T1; thus, the signal from gadolinium-enhanced tissue may be suppressed in addition to fat content. Previous studies have established that inflammatory activity can be ascertained and monitored using the signal intensity ratio (SIR) as seen on serial STIR imaging. The SIR is obtained by comparing the signal intensity from the most inflamed extraocular muscle to the reference standard. In TAO (Figure 3), signal intensity values on STIR imaging have been shown to increase proportionally to increases in disease activity, as measured by the clinical activity score (CAS).[7–10] Thus, quantifiable measures obtained via orbital imaging such as SIR values may also be valuable in disease monitoring. The measurement of T2 relaxation times of edematous extraocular muscles has also been used as a marker of disease activity following treatment, but results have been mixed.[11–13]

Diffusion-weighted imaging and ADC maps

Diffusion-weighted imaging (DWI) is a form of MRI that exploits the contrast between the random Brownian motion of water molecules. It is a measure of the extent of free molecular motion in different tissues. Within tissue, the random motion of water molecules is hindered by cell membrane boundaries as dictated by normal tissue architecture or the presence of diffusion-restricting pathological changes. DWI allows for accurate assessment of restricted diffusion via the construction of an apparent diffusion coefficient (ADC) map. ADC is a parameter calculated using MRI to quantify the magnitude of diffusion within tissue. Decreased Brownian motion, which may be caused by cellular swelling or increased density of cells, is captured on DWI as hyperintense signal. True diffusion restriction is represented by high DWI signal and corresponding low signal on the ADC map, such as in lymphoma, stroke, cytotoxic, change, or other hypercellular tumors. Areas of hyperintense DWI signal with a normal or high ADC are due to T2 „shine-through.“ In these cases, the hyperintensity on DWI is caused by the T2 signal shining through the image, rather than restricted diffusion in the tissue.[14–16]

DWI is widely used in neuroimaging as it is instrumental in identifying cytotoxic edema that occurs within minutes of stroke. Intracellular shift of fluid and contraction of the extracellular space in cytotoxic edema lead to a decrease in Brownian motion that is seen as restricted diffusion on DWI.[17] For the orbital surgeon, DWI serves as a useful tool in helping distinguish malignant from benign lesions, particularly lymphoma from benign inflammatory processes (Figure 4, Figure 5). Increased tissue density characterized by increased cellularity, larger nuclei, and relatively decreased extracellular space contribute to restricted diffusion in malignant tissue. These changes result in decreased Brownian motion of water molecules, which is captured on DWI as a hyperintense signal and reduced ADC. In contrast, most benign inflammatory lesions will demonstrate less diffusion restriction due to higher free water content and less cellular density. The increased Brownian motion results in hypointense DWI signal.

DWI is most commonly performed using a spin echo planar imaging (EPI) sequence, although other non-EPI techniques are available. EPI is typically employed due to its speed and insensitivity to motion, but it is limited by magnetic susceptibility artifact and geometric distortion. A recent study by Bae *et al.* demonstrated that in the orbit, single shot EPI and multishot EPI with fat suppression are equally effective in producing high resolution images with both minimal artifact and restricted lipid signal.[18] Non-echo planar sequences demonstrate higher resolution and thinner sections than EPI, but generally have a lower signal to noise ratio than EPI.[19] Non-EPI techniques include half-Fourier acquisition single-shot turbo spin-echo (HASTE) and multishot turbo spin-echo techniques. These techniques have been shown to be superior diagnostic and management tools to EPI in some cases.[20,21] Interestingly, recent reports have highlighted the utility of non-EPI DWI sequences in assessing treatment response in patients with TAO. As discussed above, the signal-intensity ratio (SIR) derived from STIR MRI may correlate with CAS, and signal typically reduces with treatment. Using DWI, ADC values have been shown to be significantly higher in extraocular muscles involved in active TAO. Change in ADC signal have been shown to correlate with SIR values as well as CAS and may also be used to detect subclinical changes in disease activity.[22,23]

In the orbit, DWI has been demonstrated to be particularly useful in distinguishing lymphoma from inflammatory disease such as idiopathic orbital inflammation (pseudotumor)[24–29]. The differentiation of orbital lymphoma from benign lymphoproliferative processes is essential to appropriate clinical treatment and management by the orbital surgeon. Conventional MRI is limited in its ability to differentiate malignant lymphoma from other lymphoproliferative disease.[30,31] Some studies have found features seen on MRI that differentiate benign disease from malignant lymphoma. For example, involvement of the orbit preseptal space[32] and tumor hyperintensity on T2[33] have been associated with malignant disease, while presence of “flow void sign” [28,31] or findings of sinusitis[28,32] are predictive of benign disease. However, the statistical significance of these associations may be unreliable due to variability of tumor morphology. The addition of ADC value measurement using DWI to conventional MRI studies may increase the sensitivity and specificity of radiologic diagnosis. Increased cellular density and enlargement of nuclei in orbital lymphoma leads to relative reduction in extracellular and intracellular diffusion of water molecules, thus corresponding to a decreased mean ADC value.

Multiple studies have shown that ADC values may help differentiate lymphoma from benign inflammatory orbital disease, with varying ADC cutoffs leading to different sensitivities and specificities (findings summarized in Table 1). Several studies have demonstrated the sensitivity of DWI in distinguishing benign from other malignant lesions in the orbit as well (Figure 6).[29,34] Finally, some studies have demonstrated the usefulness of DWI in distinguishing cystic from solid tumors without the use of contrast.[35] Sepahdari *et al.* analyzed data from the three largest published case series on the use of DWI in differentiating orbital lesions. The authors of this aggregate analysis determined the cutoff value of ADC $< 0.92 \times 10^{-3}$ mm^2/s differentiated lymphoma from inflammation with 100% sensitivity and specificity. ADC values were less useful in distinguishing all malignant (primarily lymphoma, metastases, rhabdomyosarcoma, carcinoma) from benign lesions.[26]

In other studies, further classification of tumor types has been analyzed based on flow patterns, particularly in pediatric tumors. However, the characterization of ADC and diffusion patterns in lesions with restricted diffusion has limited benefit due to overlap between benign and malignant lesions.[15] Additional studies comparing tumor types and inflammatory disease with DWI will help to better assess its utility in other orbital conditions.

Dynamic contrast-enhanced imaging

Dynamic contrast-enhanced (DCE) MRI is a method in which a series of images are acquired in rapid succession prior to and following the administration of contrast. It allows for the analysis of microvascular patterns of tissue perfusion. Multiple studies have shown DCE MRI to have superior diagnostic accuracy in distinguishing benign from malignant orbital lesions compared with standard MRI techniques, as well as DWI. With this technique, a region of interest is selected within the lesion for calculation of time-intensity curves (TIC) as well as various quantitative pharmacokinetic parameters (e.g. K^{trans}, v_e, K_{ep}, and v_p). Yuan *et al.* analyzed DCE images based on a washout-type TIC constructed for each of 59 untreated orbital lesions. TICs were categorized as type I or persistent pattern (steady enhancement demonstrated by a straight or curved line), type II or plateau pattern (increasing slope with plateau and final intensity at 90–100% of the peak intensity), or type III or washout pattern (rapid increasing slope and wash-out with final intensity lower than 90% of the peak). The authors found that all 26 lesions with type I persistent pattern were benign, while 10 of 14 lesions with type III washout pattern were malignant. Plateau curves (type II) were found in both benign and malignant lesions.[36]

Several recent studies have compared the accuracy of diagnostic algorithms using a combination of values obtained from DWI and DCE versus DWI alone. Most recently, Xu *et al.* used DWI and DCE MRI to evaluate 65 orbital lesions. One parameter used in DCE, K_{ep}, is the flux rate constant between the extravascular extracellular space and the plasma, may be a potential biomarker for differentiation on DCE images. In this study, malignant lesions demonstrated significantly lower ADC (cutoff value of 0.809×10^{-3} mm^2/s) and higher K_{ep} (cutoff value of 0.788/min) values than benign lesions. The authors found that the diagnostic accuracy of a combined ADC and K_{ep} index was superior to using either of the values alone (the combined modality demonstrated a sensitivity of 96.6% and specificity of 91.7%, compared to a 86.2% and 86.1% for ADC alone and 93.1% and 63.9% for K_{ep} alone).[37] These findings echoed those found by Ro *et al.* in an earlier study on 65 orbital lesions.[38]

Sun *et al.* found a significantly increased probability for differentiation of orbital lymphoma from orbital inflammation when DWI and DCE MRI were used in combination in comparison to DWI alone. The authors suggest a stepwise approach for the differentiation of lymphoma using both ADC and contrast index cutoff values. Lesions with an ADC $\leq 0.7505 \times 10^{-3}$ mm^2/s were designated as lymphoma with 76.7% sensitivity and 100% specificity. Contrast index (CI) is a parameter calculated using signal intensities measured from the DCE imaging series. The authors found that among the lesions with ADC $> 0.7505 \times 10^{-3}$ mm^2/s (which had been categorized as orbital inflammation), using a cutoff of CI ≤ 0.9686

identified additional malignant lesions. The sensitivity and specificity of using both ADC and CI cutoff values together were 90% and 87% respectively.[39]

Steady-state MRI sequences

Steady-state free precession (SSFP) sequences such as constructive interference in steady-state (e.g. CISS from Siemens, Erlangen, Germany) and fast imaging employing steady-state acquisition (e.g. FIESTA from General Electric, Milwaukee, USA or TrueFISP from Siemens) are high resolution MRI sequences in which longitudinal and transverse magnetization are maintained at a steady-state. Repetitive excitation pulses generate signal and the image constructed is based on the tissue relaxation properties. SSFP MR images allow for highly detailed three-dimensional reconstruction of tissues. SSFP sequences generate a strong signal in tissues that have a high T2/T1 ratio, such as CSF and fat. In contrast to very bright CSF, the hypointensity of even very small lesions will be evident within any structure adjacent to CSF spaces. Therefore, these sequences are valuable for distinguishing and evaluating tumors of the optic nerve (e.g. glioma) and cranial nerves (e.g. schwanomma) (Figure 7), as well as any structures in close opposition to CSF, such as the cavernous sinus and orbital apex.[40] Seitz *et al.* demonstrated the utility of CISS sequences in visualizing protrusion of the optic disc into the globe as well as clear differentiation between the orbital fat, optic nerve sheath, surrounding CSF, optic nerve, and optic chiasm in 12 patients with clinically diagnosed papilledema.[41] An additional advantage of SSFP sequences is the very short acquisition time, reducing any artifact related to CSF pulsation.[42,43] CISS sequences have been demonstrated to provide high quality visualization of most of the cranial nerves.[44,45] Yazici *et al.* used CISS MR imaging to demonstrate the formation and subsequent resolution of a fluid collection adjacent to the decompression site in the early postoperative period following optic nerve sheath decompression for idiopathic intracranial hypertension. The authors noted excellent differentiation between the optic nerve, nerve sheath, and orbital fat on the images acquired using CISS.[46]

Applications of SSFP sequences in ophthalmology are increasing. For example, recent reports have demonstrated that SSFP neuroimaging aids in identifying cranial nerve abnormalities that were radiographically diagnostic of Duane's retraction syndrome and/or Möbius syndrome (i.e. congenital cranial nerve maldevelopment).[47–49] Jiao *et al.* showed that three-dimensional FIESTA provides excellent visualization of the brainstem and the ocular motor nerves that supply the extraocular muscles and their associated connective tissues. The images were used to demonstrate various specific congenital structural abnormalities leading to strabismus.[48] Similarly, Pilyugina *et al.* used FIESTA to identify an isolated sixth cranial nerve aplasia in a young patient who had presented with reduced abduction of one eye.[49] Wani *et al.* described a case of Tolosa-Hunt syndrome causing unilateral painful ophthalmoplegia in a middle-aged woman. T2 showed a hypointense lesion in the cavernous sinus lateral to the internal carotid artery. Axial CISS imaging revealed enlargement of the cavernous sinus due to the soft tissue lesion within the sinus, which was hypointense and extended anteriorly toward the orbital apex. The diagnosis of Tolosa-Hunt syndrome was confirmed with resolution of the lesion on repeat MRI after successful treatment with steroid therapy.[42] This case demonstrates the utility of this

sequence in the precise evaluation of a soft tissue lesion in the cavernous sinus and the exclusion of vascular abnormalities.

A study by Gizewski *et al.* compared gadolinium-enhanced T1 with CISS imaging of 80 children with retinoblastoma in the evaluation of involvement of extra-retinal structures. The authors found that multiplanar reconstruction of the orbit using CISS sequences provided excellent visualization of tumor extension, aiding in pre-surgical planning. The surgeons were able to reliably interpret the exact three-dimensional tumor extension using CISS. Neuroradiologists were able to detect scleral or ciliary body infiltration. However, fat-suppressed contrast-enhanced T1 was superior to CISS in visualization of optic nerve infiltration, which changed the treatment plan and patient outcome.[50]

Dynamic MR angiography

MR angiography is a noninvasive modality used to acquire high-resolution images of dynamic blood flow. It is especially useful in evaluating and diagnosing orbital vascular lesions and, when done in conjunction with MRI, it provides superior detail about the internal soft tissue makeup of lesions compared to CT and CT angiography. Non-contrast MRA is sensitive to flow-related enhancement, and can identify arterial components of lesions. Dynamic sequences are acquired post-contrast and go by many names, such as Time-Resolved Imaging of Contrast KineticS MRA (TRICKS; GE Healthcare [Chalfont St Giles, England]), TWIST (Siemens), 4D-TRAK (Philips), TRAQ (Hitachi), and Freeze Frame (Toshiba). Using this technique, it is possible to produce a three-dimensional image of the vascularity of the region of interest over time via the passage of the contrast medium (Figure 8). The imaging protocol generally involves acquiring 20–30 three-dimensional MRA images over the region of interest in less than one minute during bolus injection of a gadolinium contrast agent. The benefits of MRA angiography compared to conventional angiography include minimal invasiveness and a better safety profile.

Kahana *et al.* described the advantage of TRICKS MRA in distinguishing between low-flow cavernous hemangioma and more hypervascular lesions such as hemangiopericytoma or highly vascular solitary fibrous tumor. The authors also highlighted a case in which TRICKS MRA aided in the evaluation of the extent of cutaneous arteriovenous malformation involving the ophthalmic, superficial temporal, and facial arteries.[51] Ramey *et al.* reported that 9 of 12 orbital lesions (75%) that underwent TRICKS MRA were correctly diagnosed by the imaging, with histopathological confirmation.[52] The utility of this technology will likely be revealed as more ophthalmologists consider MRA as a tool in the diagnosis and characterization of orbital vascular lesions.

Improvements in MRI systems

As MRI techniques advance, developments in the overall systems also allow for improved imaging resolution. One such advancement is the use of ultra-high magnetic field strength, such as 7 Tesla. Ultra-high field MRI has several advantages compared to lower field MRI, including higher signal-to-noise ratio and higher contrast-to-noise ratio. The superior resolution provided by the higher strength magnetic field produces images with greater detail of neuroanatomy, including the eye and orbit, and thus superior diagnostic

precision.[53,54] Some reports have commented on the utility of improved image quality in 7 Tesla MRI in helping distinguish fine details such as optic nerve involvement in choroidal melanoma.[53,55]

Surface coils are structures that receive radiofrequency and can be placed near the site that is being imaged to reduce artifact and improve image resolution. The use of orbital surface coils with high-resolution MRI allows for a very high level of detail of structures within the orbit.[56] This technology is useful in visualization and surgical planning for pathology involving the cranial nerves and extraocular muscles.[57–59] Sirin *et al.* used high-resolution MRI on 1.5 Tesla scanners with two orbital surface coils to detect metastatic risk factors (e.g. choroidal invasion, optic nerve infiltration) in children with retinoblastoma with high sensitivity and specificity.[60] The improved imaging resolution enabled by these advances can provide the orbital surgeon with even more detail regarding orbital disease processes and guide surgical planning.

Conclusion

Specialized MRI techniques yield sophisticated imaging data that greatly enhances diagnostic capability compared to conventional MRI. These techniques, such as diffusion weighted imaging, dynamic contrast-enhanced imaging, steady-state free precession sequences, and dynamic MR angiography, have contributed to improved methods of distinguishing benign from malignant lesions, characterization of vascular lesions, and providing more information overall to the orbital surgeon. It is essential that orbital surgeons are aware of these imaging capabilities, as they are continually evolving and are helpful in evaluation and treatment of orbital lesions as well as surgical planning when indicated. As computing power increases, along with technical advances in scanning equipment, the diagnostic accuracy and utility of MRI will no doubt increase.

Acknowledgements:

We would like to thank Rita Bhatia, MD for her assistance with the images for Figure 7.

References

1. Hoch M, Win W, Hagiwara M, Fatterpekar G, Patel S. Orbital lesions with low signal intensity on T2-weighted imaging. Clin Radiol. 2016;71(1):e88–95. [PubMed: 26602937]
2. Lee DH. Mechanisms of contrast enhancement in magnetic resonance imaging. Can Assoc Radiol J. 1991;42(1):6–12. [PubMed: 2001531]
3. Cakirer S, Cakirer D, Basak M, Durmaz S, Altuntas Y, Yigit U. Evaluation of extraocular muscles in the edematous phase of Graves ophthalmopathy on contrast-enhanced fat-suppressed magnetic resonance imaging. J Comput Assist Tomogr. 2004;28(1):80–86. [PubMed: 14716237]
4. Tien RD, Chu PK, Hesselink JR, Szumowski J. Intra- and paraorbital lesions: value of fat-suppression MR imaging with paramagnetic contrast enhancement. AJNR Am J Neuroradiol. 1991;12(2):245–253. [PubMed: 1902021]
5. Lee AG, Johnson MC, Policeni BA, Smoker WR. Imaging for neuro-ophthalmic and orbital disease - a review. Clin Exp Ophthalmol. 2009;37(1):30–53. [PubMed: 19016810]
6. Passi N, Degnan AJ, Levy LM. MR imaging of papilledema and visual pathways: effects of increased intracranial pressure and pathophysiologic mechanisms. AJNR Am J Neuroradiol. 2013;34(5):919–924. [PubMed: 22422187]

7. Mayer E, Herdman G, Burnett C, Kabala J, Goddard P, Potts MJ. Serial STIR magnetic resonance imaging correlates with clinical score of activity in thyroid disease. Eye (Lond). 2001;15(Pt 3):313–318. [PubMed: 11450728]
8. Mayer EJ, Fox DL, Herdman G, et al. Signal intensity, clinical activity and cross-sectional areas on MRI scans in thyroid eye disease. Eur J Radiol. 2005;56(1):20–24. [PubMed: 15896938]
9. Tortora F, Cirillo M, Ferrara M, et al. Disease activity in Graves' ophthalmopathy: diagnosis with orbital MR imaging and correlation with clinical score. Neuroradiol J. 2013;26(5):555–564. [PubMed: 24199816]
10. Higashiyama T, Iwasa M, Ohji M. Quantitative Analysis of Inflammation in Orbital Fat of Thyroid-associated Ophthalmopathy Using MRI Signal Intensity. Sci Rep. 2017;7(1):16874. [PubMed: 29203853]
11. Prummel MF, Gerding MN, Zonneveld FW, Wiersinga WM. The usefulness of quantitative orbital magnetic resonance imaging in Graves' ophthalmopathy. Clin Endocrinol (Oxf). 2001;54(2):205–209. [PubMed: 11207635]
12. Tachibana S, Murakami T, Noguchi H, et al. Orbital magnetic resonance imaging combined with clinical activity score can improve the sensitivity of detection of disease activity and prediction of response to immunosuppressive therapy for Graves' ophthalmopathy. Endocr J. 2010;57(10):853–861. [PubMed: 20733265]
13. Das T, Roos JCP, Patterson AJ, Graves MJ, Murthy R. T2-relaxation mapping and fat fraction assessment to objectively quantify clinical activity in thyroid eye disease: an initial feasibility study. Eye (Lond). 2019;33(2):235–243. [PubMed: 30538310]
14. Baliyan V, Das CJ, Sharma R, Gupta AK. Diffusion weighted imaging: Technique and applications. World J Radiol. 2016;8(9):785–798. [PubMed: 27721941]
15. Lope LA, Hutcheson KA, Khademian ZP. Magnetic resonance imaging in the analysis of pediatric orbital tumors: utility of diffusion-weighted imaging. J aapos. 2010;14(3):257–262. [PubMed: 20603060]
16. Griffin AS, Hoang JK, Malinzak MD. CT and MRI of the Orbit. Int Ophthalmol Clin. 2018;58(2):25–59.
17. Kanekar SG, Zacharia T, Roller R. Imaging of stroke: Part 2, Pathophysiology at the molecular and cellular levels and corresponding imaging changes. AJR Am J Roentgenol. 2012;198(1):63–74. [PubMed: 22194480]
18. Bae YJ, Choi BS, Jeong HK, Sunwoo L, Jung C, Kim JH. Diffusion-Weighted Imaging of the Head and Neck: Influence of Fat-Suppression Technique and Multishot 2D Navigated Interleaved Acquisitions. AJNR Am J Neuroradiol. 2018;39(1):145–150. [PubMed: 29122759]
19. Dudau C, Draper A, Gkagkanasiou M, Charles-Edwards G, Pai I, Connor S. Cholesteatoma: multishot echo-planar vs non echo-planar diffusion-weighted MRI for the prediction of middle ear and mastoid cholesteatoma. BJR|Open. 2019;1(1):20180015. [PubMed: 33178911]
20. Khemani S, Singh A, Lingam RK, Kalan A. Imaging of postoperative middle ear cholesteatoma. Clin Radiol. 2011;66(8):760–767. [PubMed: 21524417]
21. Lingam RK, Khatri P, Hughes J, Singh A. Apparent diffusion coefficients for detection of postoperative middle ear cholesteatoma on non-echo-planar diffusion-weighted images. Radiology. 2013;269(2):504–510. [PubMed: 23801772]
22. Ritchie AE, Lee V, Feeney C, Lingam RK. Using Nonechoplanar Diffusion-weighted MRI to Assess Treatment Response in Active Graves Orbitopathy: A Novel Approach with 2 Case Reports. Ophthalmic Plast Reconstr Surg. 2016;32(3):e67–70. [PubMed: 25141074]
23. Lingam RK, Mundada P, Lee V. Novel use of non-echo-planar diffusion weighted MRI in monitoring disease activity and treatment response in active Grave's orbitopathy: An initial observational cohort study. Orbit. 2018;37(5):325–330. [PubMed: 29319381]
24. Kapur R, Sepahdari AR, Mafee MF, et al. MR imaging of orbital inflammatory syndrome, orbital cellulitis, and orbital lymphoid lesions: the role of diffusion-weighted imaging. AJNR Am J Neuroradiol. 2009;30(1):64–70. [PubMed: 18842758]
25. Roshdy N, Shahin M, Kishk H, et al. MRI in diagnosis of orbital masses. Curr Eye Res. 2010;35(11):986–991. [PubMed: 20958187]

26. Sepahdari AR, Politi LS, Aakalu VK, Kim HJ, Razek AA. Diffusion-weighted imaging of orbital masses: multi-institutional data support a 2-ADC threshold model to categorize lesions as benign, malignant, or indeterminate. AJNR Am J Neuroradiol. 2014;35(1):170–175. [PubMed: 23868150]
27. Politi LS, Forghani R, Godi C, et al. Ocular adnexal lymphoma: diffusion-weighted mr imaging for differential diagnosis and therapeutic monitoring. Radiology. 2010;256(2):565–574. [PubMed: 20656841]
28. Haradome K, Haradome H, Usui Y, et al. Orbital lymphoproliferative disorders (OLPDs): value of MR imaging for differentiating orbital lymphoma from benign OPLDs. AJNR Am J Neuroradiol. 2014;35(10):1976–1982. [PubMed: 24874530]
29. Razek AA, Elkhamary S, Mousa A. Differentiation between benign and malignant orbital tumors at 3-T diffusion MR-imaging. Neuroradiology. 2011;53(7):517–522. [PubMed: 21286695]
30. Akansel G, Hendrix L, Erickson BA, et al. MRI patterns in orbital malignant lymphoma and atypical lymphocytic infiltrates. Eur J Radiol. 2005;53(2):175–181. [PubMed: 15664279]
31. Xu XQ, Hu H, Liu H, et al. Benign and malignant orbital lymphoproliferative disorders: Differentiating using multiparametric MRI at 3.0T. J Magn Reson Imaging. 2017;45(1):167–176. [PubMed: 27299917]
32. Ren J, Yuan Y, Wu Y, Tao X. Differentiation of orbital lymphoma and idiopathic orbital inflammatory pseudotumor: combined diagnostic value of conventional MRI and histogram analysis of ADC maps. BMC Med Imaging. 2018;18(1):6. [PubMed: 29716527]
33. Cytryn AS, Putterman AM, Schneck GL, Beckman E, Valvassori GE. Predictability of magnetic resonance imaging in differentiation of orbital lymphoma from orbital inflammatory syndrome. Ophthalmic Plast Reconstr Surg. 1997;13(2):129–134. [PubMed: 9185195]
34. Sepahdari AR, Aakalu VK, Setabutr P, Shiehmorteza M, Naheedy JH, Mafee MF. Indeterminate orbital masses: restricted diffusion at MR imaging with echo-planar diffusion-weighted imaging predicts malignancy. Radiology. 2010;256(2):554–564. [PubMed: 20656840]
35. Hiwatashi A, Togao O, Yamashita K, et al. High Resolution Diffusion-Weighted Imaging for Solitary Orbital Tumors : 3D Turbo Field Echo with Diffusion-Sensitized Driven-Equilibrium (DSDE-TFE) Preparation Technique. Clin Neuroradiol. 2018;28(2):261–266. [PubMed: 28097371]
36. Yuan Y, Kuai XP, Chen XS, Tao XF. Assessment of dynamic contrast-enhanced magnetic resonance imaging in the differentiation of malignant from benign orbital masses. Eur J Radiol. 2013;82(9):1506–1511. [PubMed: 23561057]
37. Xu XQ, Qian W, Ma G, et al. Combined diffusion-weighted imaging and dynamic contrast-enhanced MRI for differentiating radiologically indeterminate malignant from benign orbital masses. Clin Radiol. 2017;72(10):903.e909–903.e915.
38. Ro SR, Asbach P, Siebert E, Bertelmann E, Hamm B, Erb-Eigner K. Characterization of orbital masses by multiparametric MRI. Eur J Radiol. 2016;85(2):324–336. [PubMed: 26781137]
39. Sun B, Song L, Wang X, et al. Lymphoma and inflammation in the orbit: Diagnostic performance with diffusion-weighted imaging and dynamic contrast-enhanced MRI. J Magn Reson Imaging. 2017;45(5):1438–1445. [PubMed: 27649521]
40. Stuckey SL, Harris AJ, Mannolini SM. Detection of acoustic schwannoma: use of constructive interference in the steady state three-dimensional MR. AJNR Am J Neuroradiol. 1996;17(7):1219–1225. [PubMed: 8871702]
41. Seitz J, Held P, Strotzer M, et al. Magnetic resonance imaging in patients diagnosed with papilledema: a comparison of 6 different high-resolution T1- and T2(*)-weighted 3-dimensional and 2-dimensional sequences. J Neuroimaging. 2002;12(2):164–171. [PubMed: 11977913]
42. Wani NA, Jehangir M, Lone PA. Tolosa-Hunt Syndrome Demonstrated by Constructive Interference Steady State Magnetic Resonance Imaging. J Ophthalmic Vis Res. 2017;12(1):106–109. [PubMed: 28299013]
43. Sheth S, Branstetter BFt, Escott EJ. Appearance of normal cranial nerves on steady-state free precession MR images. Radiographics. 2009;29(4):1045–1055. [PubMed: 19605655]
44. Yousry I, Camelio S, Schmid UD, et al. Visualization of cranial nerves I-XII: value of 3D CISS and T2-weighted FSE sequences. Eur Radiol. 2000;10(7):1061–1067. [PubMed: 11003398]

45. Held P, Nitz W, Seitz J, et al. Comparison of 2D and 3D MRI of the optic and oculomotor nerve anatomy. Clin Imaging. 2000;24(6):337–343. [PubMed: 11368933]
46. Yazici Z, Yazici B, Tuncel E. Findings of magnetic resonance imaging after optic nerve sheath decompression in patients with idiopathic intracranial hypertension. Am J Ophthalmol. 2007;144(3):429–435. [PubMed: 17640608]
47. Wu SQ, Man FY, Jiao YH, Xian JF, Wang YD, Wang ZC. Magnetic resonance imaging findings in sporadic Mobius syndrome. Chin Med J (Engl). 2013;126(12):2304–2307. [PubMed: 23786943]
48. Jiao YH, Zhao KX, Wang ZC, et al. Magnetic resonance imaging of the extraocular muscles and corresponding cranial nerves in patients with special forms of strabismus. Chin Med J (Engl). 2009;122(24):2998–3002. [PubMed: 20137490]
49. Pilyugina SA, Fischbein NJ, Liao YJ, McCulley TJ. Isolated sixth cranial nerve aplasia visualized with Fast Imaging Employing Steady-State Acquisition (FIESTA) MRI. J Neuroophthalmol. 2007;27(2):127–128. [PubMed: 17548999]
50. Gizewski ER, Wanke I, Jurklies C, Gungor AR, Forsting M. T1 Gd-enhanced compared with CISS sequences in retinoblastoma: superiority of T1 sequences in evaluation of tumour extension. Neuroradiology. 2005;47(1):56–61. [PubMed: 15650830]
51. Kahana A, Lucarelli MJ, Grayev AM, Van Buren JJ, Burkat CN, Gentry LR. Noninvasive dynamic magnetic resonance angiography with Time-Resolved Imaging of Contrast KineticS (TRICKS) in the evaluation of orbital vascular lesions. Arch Ophthalmol. 2007;125(12):1635–1642. [PubMed: 18071114]
52. Ramey NA, Lucarelli MJ, Gentry LR, Burkat CN. Clinical usefulness of orbital and facial Time-Resolved Imaging of Contrast KineticS (TRICKS) magnetic resonance angiography. Ophthalmic Plast Reconstr Surg. 2012;28(5):361–368. [PubMed: 22836799]
53. Obusez EC, Lowe M, Oh SH, et al. 7T MR of intracranial pathology: Preliminary observations and comparisons to 3T and 1.5T. Neuroimage. 2018;168:459–476. [PubMed: 27915116]
54. Lindner T, Langner S, Graessl A, et al. High spatial resolution in vivo magnetic resonance imaging of the human eye, orbit, nervus opticus and optic nerve sheath at 7.0 Tesla. Exp Eye Res. 2014;125:89–94. [PubMed: 24928314]
55. Singh AD, Platt SM, Lystad L, et al. Optic Nerve Assessment Using 7-Tesla Magnetic Resonance Imaging. Ocul Oncol Pathol. 2016;2(3):178–180. [PubMed: 27239461]
56. Georgouli T, Chang B, Nelson M, et al. Use of high-resolution microscopy coil MRI for depicting orbital anatomy. Orbit. 2008;27(2):107–114. [PubMed: 18415870]
57. Gupta C, Sharma P, Saxena R, Garg A, Sharma S. Clinical correlation of imaging findings in congenital cranial dysinnervation disorders involving abducens nerve. Indian J Ophthalmol. 2017;65(2):155–159. [PubMed: 28345573]
58. Rajab GZ, Suh SY, Demer JL. Magnetic resonance imaging in dissociated strabismus complex demonstrates generalized hypertrophy of rectus extraocular muscles. J aapos. 2017;21(3):205–209. [PubMed: 28499843]
59. Oatts JT, Kumar RN, Nyong'o OL. Orbital surface coil imaging predicts surgical anatomy of medial rectus muscle in consecutive exotropia: a case report. J aapos. 2016;20(5):449–450. [PubMed: 27208854]
60. Sirin S, Schlamann M, Metz KA, et al. High-resolution MRI using orbit surface coils for the evaluation of metastatic risk factors in 143 children with retinoblastoma: Part 2: new vs. old imaging concept. Neuroradiology. 2015;57(8):815–824. [PubMed: 25964026]
61. ElKhamary SM, Galindo-Ferreiro A, AlGhafri L, Khandekar R, Schellini SA. Characterization of diffuse orbital mass using Apparent diffusion coefficient in 3-tesla MRI. Eur J Radiol Open. 2018;5:52–57. [PubMed: 29719859]

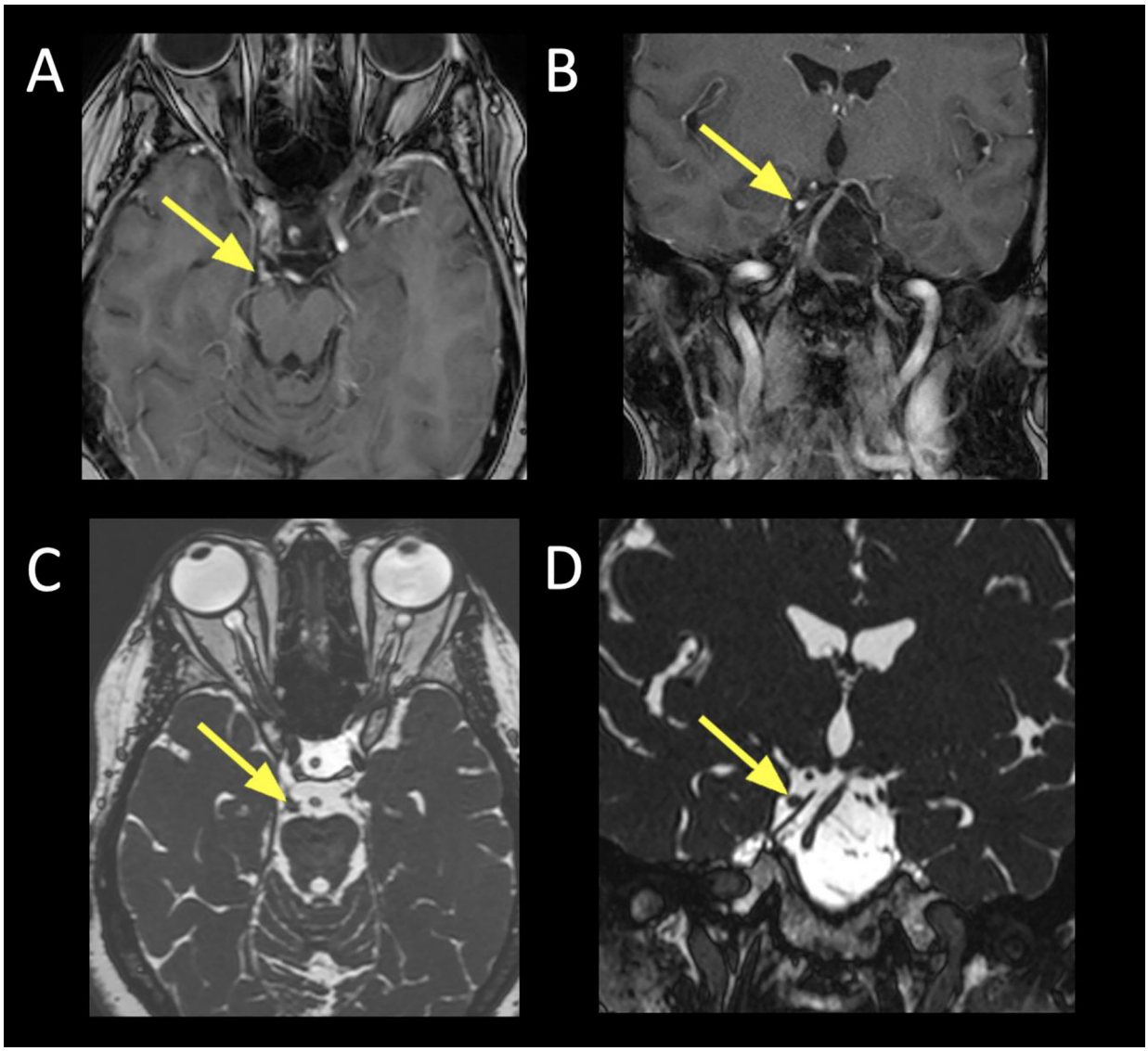

Figure 1:
Idiopathic orbital inflammation.

A. Coronal T1+C FS showing primarily superolateral extraconal inflammatory signal in the left orbit (arrow). This is contiguous to the adjacent lacrimal gland and obscures the margins along the adjacent superior and lateral recti. Small volume extension of inflammatory stranding into the lateral intraconal space.

B. Axial T1+C FS showing inflammatory mass-like signal along the left lateral rectus (arrow), extending from the lacrimal fossa toward the orbital apex.

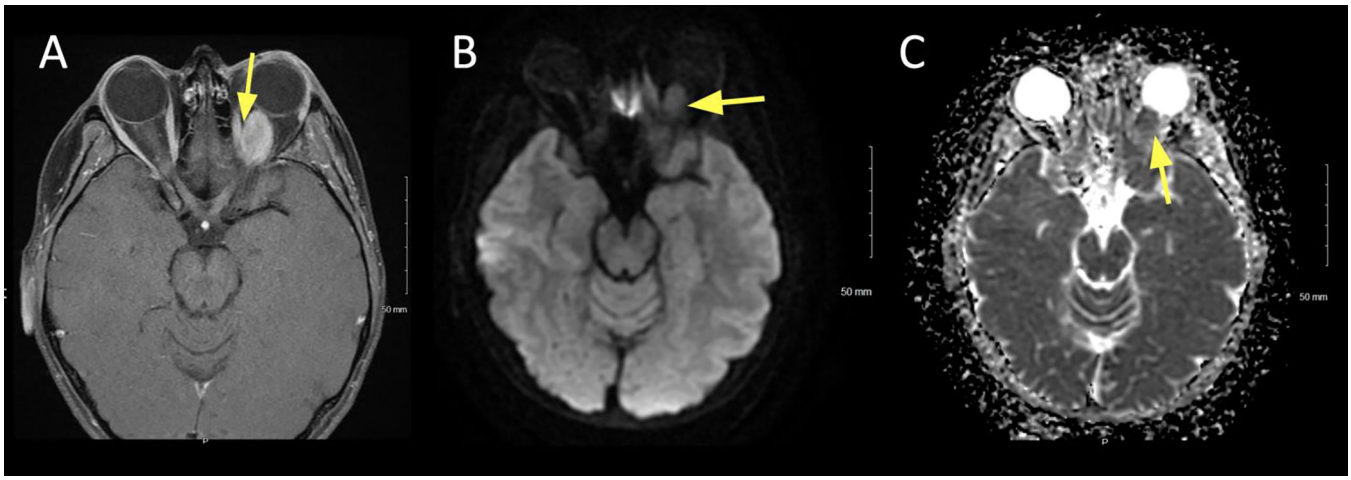

Figure 2:

A 29 year old female presented with headache. Fundus exam revealed bilateral papilledema. A lumbar puncture was performed; opening pressure was 55 cm CSF.

A. Axial T2 FS showing bilateral flattening of the posterior sclera and protrusion of the optic nerve papillae into the vitreous space of the globe (arrow).

B. Axial T1+C FS showing bilateral enhancement at the papillae (arrow).

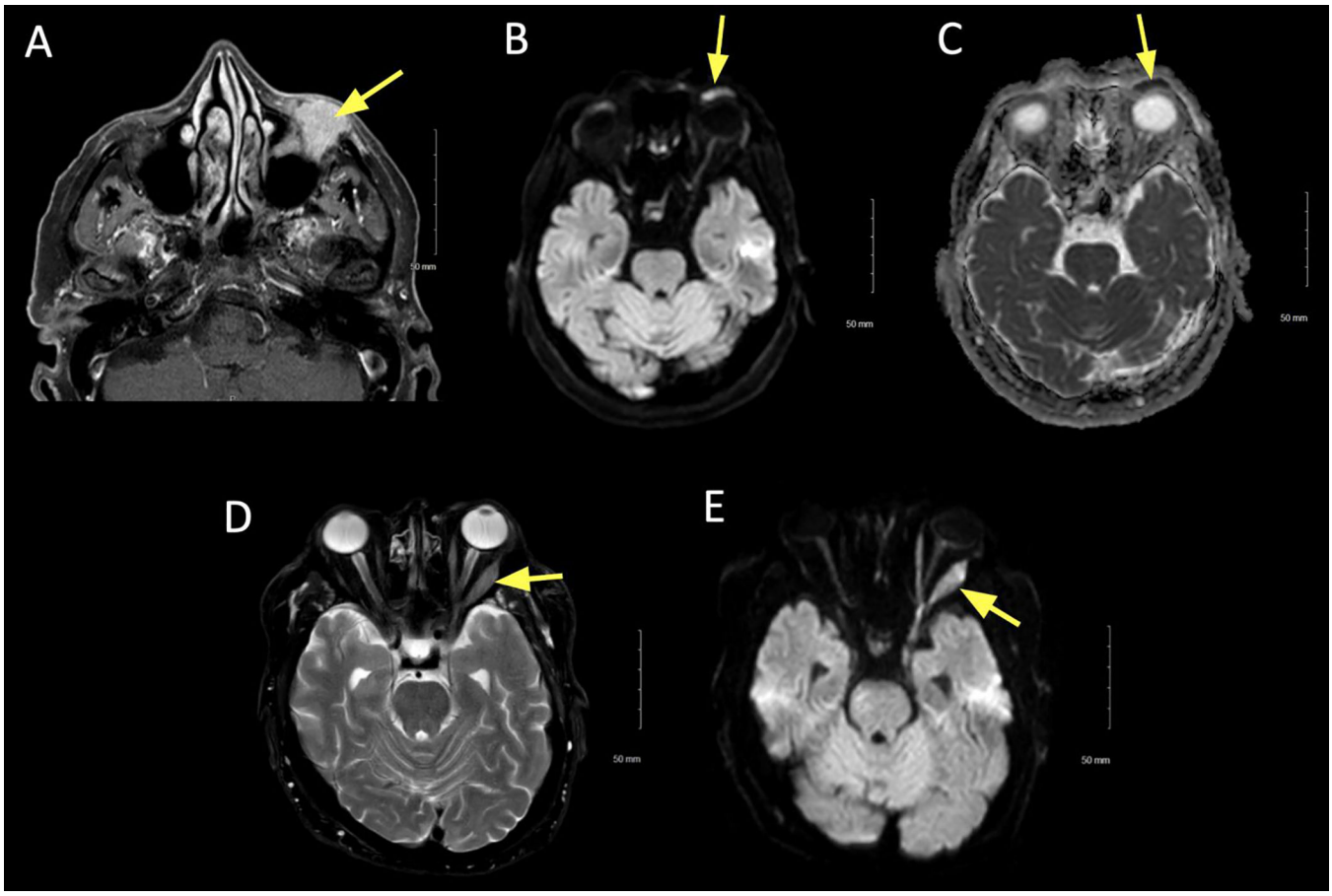

Figure 3:

Active thyroid-associated orbitopathy.

A. Coronal T1 pre contrast showing extraocular muscle enlargement without fatty infiltration (arrow).

B. Coronal T1+C FS showing extraocular muscle enlargement and enhancement (arrow).

C. Coronal STIR showing bilateral extraocular muscle enlargement and associated edema (arrow), suggesting an active process.

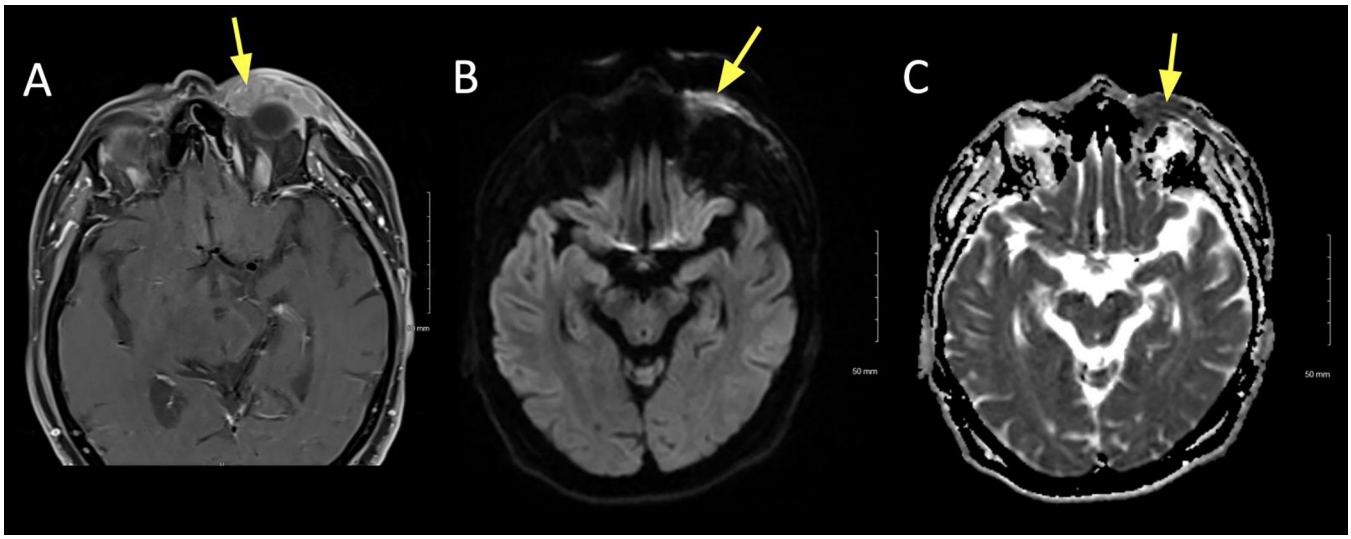

Figure 4:

A 79 year old female presented with slowly enlarging left upper and lower eyelid lesions over the past year. Diffusion weighted imaging (DWI) showed hyperintense signal, suggesting a hypercellular lesion. Biopsy confirmed mucosa-associated lymphoid tissue (MALT) lymphoma.

A. Axial T1+C FS at the superior lid level showing uniform contrast enhancement of the left upper lid (arrow).

B. Axial DWI showing hyperintense signal in the left upper lid.

C. ADC map of the lesion showing corresponding hypointense signal, signifying true restricted diffusion.

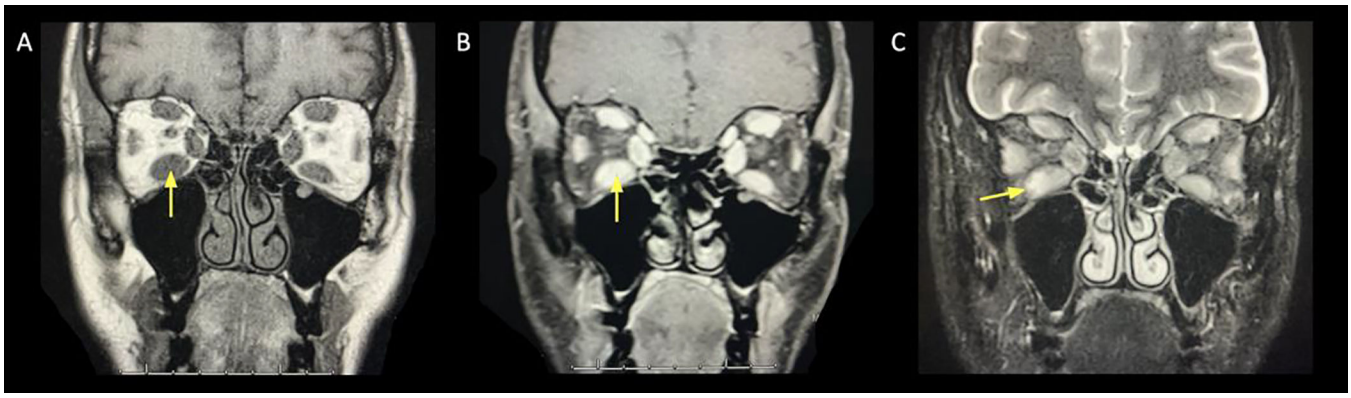

Figure 5:

A 77 year old female presented with progressively enlarging left lower eyelid lesion. Diffusion restricted imaging (DWI) was hyperintense, suggesting hypercellularity of the lesion. Biopsy was consistent with atypical lymphoid infiltrate.

A. Axial T1+C FS image showing left lower lid uniform contrast enhancement (arrow).

B. Axial DWI revealing hyperintense signal (arrow).

C. ADC map revealing corresponding hypointense signal (arrow), signifying true diffusion restriction.

D. Axial T2 FS at the mid orbit showing expansion of the left lateral rectus, with associated hypointense signal (arrow).

E. DWI showing hyperintense signal (arrow) in the left lateral rectus. Features suggest an additional site of lymphoid tissue infiltrate.

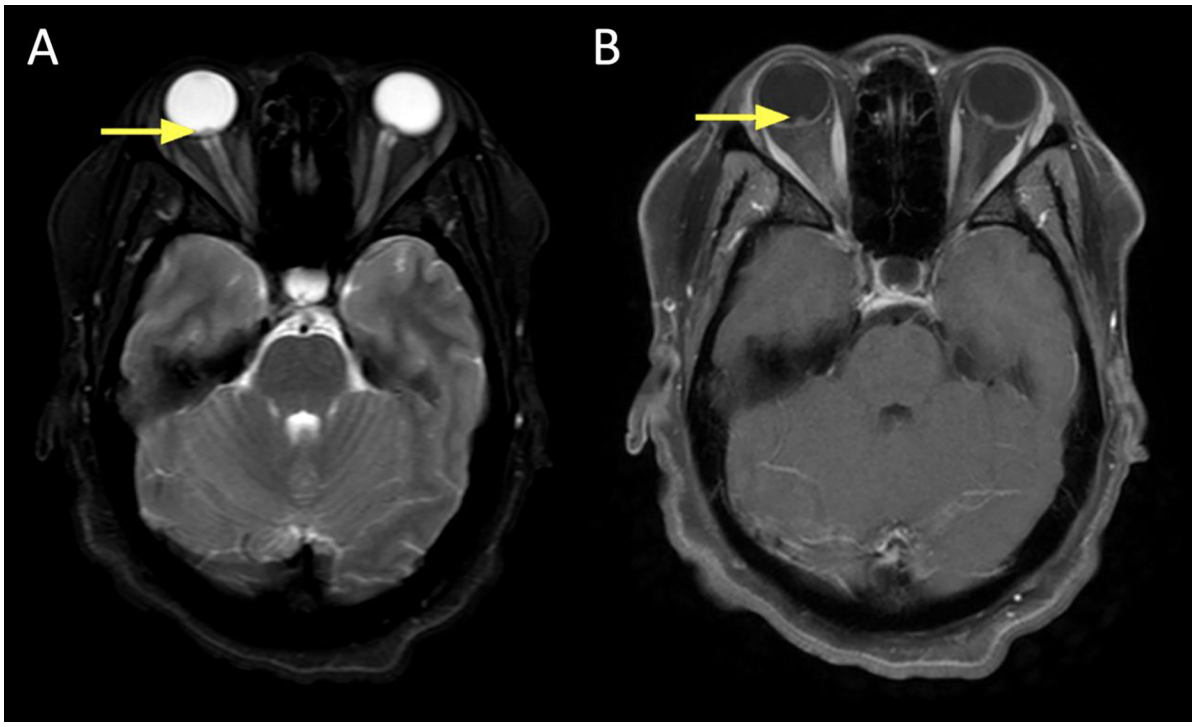

Figure 6:

A 41 year old male presented with left-sided ptosis, dysmotility, and orbital mass causing compressive optic neuropathy. Biopsy was consistent with granular cell tumor.

A. Axial T1+C FS at the mid/upper orbit reveals avid and uniform contrast enhancement of the lesion, which marginates the left medial rectus (yellow).

B. Axial DWI revealing intermediate signal in the lesion (arrow).

C. ADC map revealing slightly low signal in the lesion (arrow).

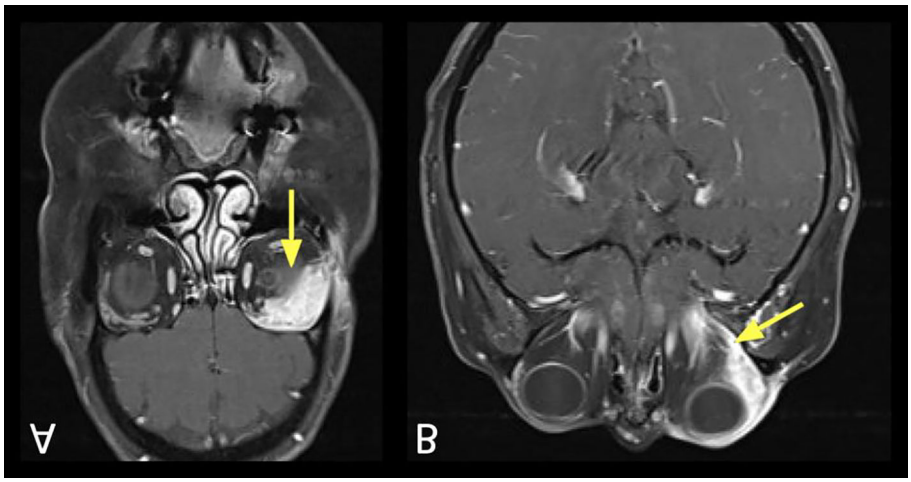

Figure 7:

Visualization of CN III schwannoma using constructive interference in steady-state (CISS) sequences.

A. Axial T1+C FS showing an enhancing lesion corresponding to the cisternal segment of CN III (arrow), just anterior to the right cerebral peduncle.

B. Coronal T1+C FS showing the same right CN III schwannoma (arrow) at the cisternal segment.

C. Axial CISS showing the filling defect (arrow) corresponding to the enlarged right CN III. Non-contrast techniques can be used to screen for lesions, and follow known lesions over time.

D. Coronal reformatted image from source axial CISS acquisition showing the right CN III, similar to the coronal contrast sequence (Figure 7B).

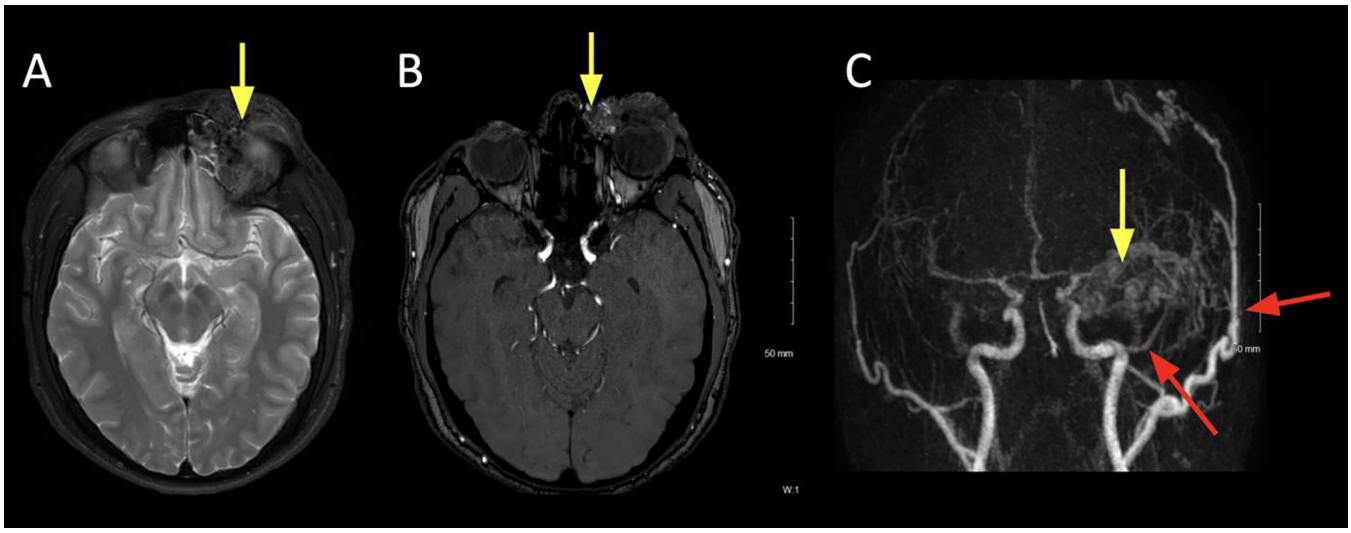

Figure 8:

A 19 year old male presented with left upper lid swelling, ptosis, and obscuring upward gaze. A bulging, reddish mass with a faint thrill was palpable.

A. Axial T2 FS at the level of the superior orbit showing expanded left upper lid and frontal brow soft tissues with tubular T2 hypointense flow voids (arrow).

B. Axial non-contrast time-of-flight (TOF) MRA at the level of the lenses showing flow related enhancement within the left medial canthal soft tissue lesion, suggestive of an arterial component (arrow)

C. Coronal maximum intensity projections (MIP) from TRICKS MRA, showing multiple regions of enhancement within the left brow lesion. This image is from the early arterial phase, showing the early arterial component within the brow (yellow arrow) and supply from hypertrophied ophthalmic (ICA) and superficial temporal arteries (ECA) branches (red arrows).

Table 1:

Use of DWI in differentiating orbital lesions

Key study endpoint	Author	Year of publication	DWI technique used	Inclusion	ADC cutoff value (x 10^{-3} mm^2/s)	Sensitivity (%)	Specificity (%)
Identification of lymphoma	Haradome *et al.*[28]	2014	Unspecified	Lymphoma (29) Benign orbital lymphoproliferative disorder (18)	< 0.612	94.1	93.3
	Politi *et al.*[27]	2010	Unspecified	Lymphoma (38) Normal orbit (18)	< 0.775	96	93
				Primary non-lymphoma neoplasm (20) Benign vascular lesion (15) Benign inflammatory lesion (12) Metastasis (11)			
	Sepahdari *et al.*[34]	2010	EPI	Lymphoma (6) Inflammatory pseudotumor (10)	< 1.0	100	100
Differentiation of malignant vs. benign lesions	ElKhamary *et al.*[61]	2018	EPI		< 0.8	86.7	66.9
	Razek *et al.*[29]	2011	EPI	Malignant (22): Non-Hodgkin lymphoma (6) Metastasis (5) Rhabdomyosarcoma (4) Adenocarcima (2) Other (5) Benign (25): Pseudotumor (5) Lymphangioma (3) Pleomorphic adenoma (3) Schwanoma (3) Venous malformation (3) Other (8)	< 1.15	95	91
	Sepahdari *et al.*[34]	2010	EPI	Malignant (16) Benign (31) (otherwise unspecified)	< 1.0	63	84

DWI: Diffusion-weighted imaging

ADC: Apparent diffusion coefficient

EPI: Echo-planar imaging